Excited states of hydrogenic impurities in quantum wells in magnetic fields

1995 J. Phys.: Condens. Matter 7 3577

(http://iopscience.iop.org/0953-8984/7/18/021)

J. Phys.: Condens. Matter 7 (1995) 3577–3590. Printed in the UK

Excited states of hydrogenic impurities in quantum wells in magnetic fields

R Chen†§, J P Cheng†‖, D L Lin†, Bruce D McCombe† and Thomas F George‡

† Department of Physics, State University of New York at Buffalo, Buffalo, NY 14260-1500, USA

‡ Departments of Physics and Chemistry, Washington State University, Pullman, WA 99164, USA

Received 22 November 1994

Abstract. Quasi-two-dimensional hydrogenic impurity levels in quantum wells under the influence of magnetic fields are investigated. Experimentally, $1s \rightarrow np$ ($n = 2, 3, 4$) transition energies in quantum wells of various widths are measured by the photoconductivity technique for magnetic fields up to 9 T. Theoretically, these energies are calculated by a new variational method that is valid for the whole range of magnetic field strengths, from the zero-field limit to the high-field limit. Good agreement is achieved for every transition for well widths up to ~ 300 Å, for which the confinement effect is appreciable. Consistent discrepancies found for 450 Å are expected to be accounted for by including subband mixing because of the wide width and small subband separation. Our study demonstrates that the simple variational method can produce good results for highly excited levels in magnetic fields provided that the confinement due to the quantum well is sufficiently strong.

1. Introduction

There has been a considerable amount of work in recent years devoted to the study of shallow impurity states in multiple quantum well (MQW) structures in a magnetic field [1–10]. Variational calculations, however, have been limited primarily to lowest levels such as 1s and $2p_{\pm 1}$ in the usual spectroscopic notation. Experimental measurements of the $1s \rightarrow 2p_{\pm 1}$ transitions yield good agreement with calculations over a wide range of well widths [11].

In the past, higher excited impurity states were mostly calculated for impurities either unconfined in the presence of arbitrary magnetic fields [12–15] or in a quantum well in the absence of magnetic fields [16]. In a magnetic field of arbitrary strength, impurity levels have been computed only for a strictly two-dimensional (2D) case [17, 18]. It is found that higher excited states behave qualitatively differently in the 2D case from the corresponding 3D states. More recently, a calculation of donor excited states in an infinite square well in arbitrary magnetic fields has been carried out by diagonalizing the Hamiltonian in Landau level–subband level product basis states [19]. Another numerical diagonalization procedure has also been introduced to identify shallow-donor impurity states in GaAs/GaAlAs MQWs

§ Present address: Department of Physics, Emory University, Atlanta, GA 30322, USA.

‖ Present address: Francis Bitter National Magnet Laboratory, Massachusetts Institute of Technology, Cambridge, MA 02139, USA.

0953-8984/95/183577+14$19.50

in moderate magnetic fields [20]. The convergence usually worsens when one goes to higher excited states.

Recently, a new variational approach has been developed by the present authors to calculate energy levels of a hydrogenic impurity up to the 4p state in a quantum well with arbitrary magnetic fields applied in the direction of growth [21]. The trial wave functions are constructed on the basis of correspondence rules [22] between low-field states and high-field states under strong confinement. For a $GaAs/Al_{0.7}Ga_{0.3}As$ MQW system with donor impurities doped at the centre of a GaAs well of width 125 Å, $1s \rightarrow np$ transition energies with $n = 2, 3, 4$ have been measured by the photoconductivity technique in magnetic fields up to 9 T [22]. Good agreement between the theory and experiments is obtained for all observed transitions [21].

Our method of calculation differs from the usual variational calculation mainly in two aspects. First, for every quasi-two-dimensional (Q2D) hydrogenic state, the trial wave function is constructed with only two independent variational parameters. Therefore, higher excited states can be handled in the same simple and straightforward manner. Second, each trial wave function yields correct wave functions in the limit of zero magnetic field as well as in the strong-field limit, provided that the confinement is sufficiently strong. The energy spectra obtained for the whole range of magnetic field strength change smoothly throughout the intermediate fields. Although there is no intention to compete in accuracy with sophisticated numerical computations in the literature, the method provides a unified picture of the energy spectrum of a confined donor impurity over a wide range of states with reasonably good accuracy.

As our trial wave functions are based on the behaviour of the system under strong confinement, it is of great interest to investigate the validity of the method when the well width increases. In addition, the subband separation decreases as the width of a quantum well increases. As a consequence, the excited states associated with higher subbands become accessible for far-infrared (FIR) optical measurements without complications of the reststrahlen band and resonant electron–LO phonon interactions, facilitating a simple comparison with the theoretical calculation.

We present in this article a study, both theoretical and experimental, of highly excited states of hydrogenic donor impurities doped at the centre of quantum wells of a wide range of different widths in a variable magnetic field. Our purpose is to investigate the validity of the variational wave functions as the well width increases and to study the change of energy level scheme as the width narrows down. In section 2, we outline how a Q2D impurity state evolves from the zero-magnetic-field limit continuously to the high-field limit, and how trial wave functions are constructed. Properties of these functions are also examined. The procedure of numerical computation is outlined in section 3, in which the calculated energy spectra as functions of the applied field for different widths are presented. In section 4, we first describe relevant experimental details, and then compare the measured transition energies with theoretical results obtained in section 3. Interesting features of our results are discussed in detail in section 5 along with a few concluding remarks.

2. Trial wave functions

The trial wave functions that guarantee correct behaviour at the zero-field end and in the high-field limit are constructed on the basis of the correspondence rules discussed in [22]. An outline of the procedure can be found in [21]. To avoid repetition, we simply write down the wave functions in the two limits and refer the readers to these two references for the notation.

For a hydrogenic impurity situated at the centre of the quantum well of width d and height V_0, under the influence of a magnetic field B in the z direction or the growing direction, we can write the wave function as

$$\Psi(\rho, z) = \left(1/\sqrt{2\pi}\right) e^{im\phi}\psi(\rho, z) \tag{1}$$

where m is an integer, and $\psi(\rho, z)$ satisfies the equation

$$[-\nabla^2 - 2w/\rho + m\gamma - \tfrac{1}{4}\gamma^2\rho^2 + V_B(z) + H']\psi = E\psi \tag{2}$$

where V_B is the confinement potential. In (2), we have introduced the operator

$$H' = 2w/\rho - 2/r \tag{3}$$

which may be treated as a perturbation in the 2D limit [1]. The parameter w is to be determined by the variational principle.

In the case of weak fields with strong confinement, (2) can be solved exactly by neglecting H' and the γ^2 term. The energy eigenvalue is simply the sum of that of a 2D hydrogenic atom with its potential modified by w, a free particle in the square well or the subband energy E_i and the Zeeman splitting of the electronic level due to the field. The corresponding eigenfunction is given by

$$\psi^w_{\nu,m,i} = \phi_{\nu,m}(\rho, w) f_i(z) \tag{4}$$

where $\psi_{\nu,m}(\rho, w)$ is the well known 2D hydrogenic wave function and $f_i(z)$ the ith subband wave function. The latter is given by

$$f_i(z) = \begin{cases} C\cos(k_z z) & |z| \leqslant d/2 \\ C\cos(k_z d/2)\exp[-k_z'(|z| - d/2)] & |z| > d/2 \end{cases} \tag{5}$$

for odd i and

$$f_i(z) = \begin{cases} C\sin(k_z z) & |z| \leqslant d/2 \\ \mathrm{sgn}(z) C\sin(k_z d/2)\exp[-k_z'(|z| - d/2)] & |z| > d/2 \end{cases} \tag{6}$$

for even i. The renormalization constant in these equations is

$$C = \sqrt{2k_z'/(k_z' + 1/d)} \tag{7}$$

and $k_z = \sqrt{2m^* E_i}/\hbar$, $k_z' = \sqrt{2m^*(V_0 - E_i)}/\hbar$. The subband energy E_i is determined by

$$(E_i/V_0)^{1/2} = \begin{cases} \left|\cos\left(\sqrt{E_i}d/2\right)\right| & \text{for odd } i \\ \left|\sin\left(\sqrt{E_i}d/2\right)\right| & \text{for even } i. \end{cases} \tag{8}$$

The function sgn(z) is 1 for positive z and -1 for negative z.

In the limit of high magnetic field with strong confinement, the Coulomb term $-2w/\rho$ in (2) can be treated as a small perturbation. The unperturbed states are then Landau levels described by the equation

$$[-\nabla^2 + m\gamma - \tfrac{1}{4}\gamma^2\rho^2 + V_B(z)]\psi_{N,m,i}(\rho, z) = E\psi_{N,m,i}(\rho, z) \tag{9}$$

which is also exactly soluble. The solutions are [23]

$$E_{N,m,i} = (2N + 1)\gamma + E_i \tag{10}$$

$$\psi_{N,m,i}(\rho, z) = \phi_{N,m}(\rho) f_i(z) \tag{11}$$

where $\phi_{N,m}(\rho)$ are the Landau level wave functions

$$\phi_{N,m}(\rho) = \{(\gamma/2\pi)\lambda!/[(\lambda + |m|)!]^3\}(\gamma\rho^2/2)^{|m|/2} \exp(-\gamma\rho^2/4) L_{\lambda+|m|}^{|m|}(\gamma\rho^2/2). \tag{12}$$

The index λ in (12) is defined by

$$\lambda = N - \tfrac{1}{2}(m + |m|). \tag{13}$$

In the absence of the magnetic field, it has been shown [22] on the basis of the concept of parity and nodal surface conservation that a one-to-one correspondence between hydrogenic wave functions for 2D and 3D cases can be established without ambiguity by the rules

$$n - \ell - 1 \to \nu - |m| - 1 \tag{14}$$

$$\ell - |m| \to i - 1. \tag{15}$$

These rules hold true for any level and are completely consistent with the non-crossing rule proposed earlier in the literature [24]. The correspondence between low-field states and high-field states can also be established in the limit of strong confinement by the parity conservation, and the rule is

$$N \to (\nu - 1) + \tfrac{1}{2}(m - |m|). \tag{16}$$

With the help of these correspondence rules, we propose the trial wave function

$$\Psi_{n,\ell,m} = \left(1/\sqrt{2\pi}\right) e^{im\phi}[\alpha\psi^{w}_{\nu,m,i} + \beta\psi_{N,m,i}] \tag{17}$$

where ν, N and i are related to n, ℓ and m by (14)–(16).

3. The energy level spectrum

The trial functions (17) involve three parameters, but only two are independent. The normalization condition eliminates one of them by the relation

$$\beta = -\alpha|S(w)| + \sqrt{\alpha^2(|S(w)|^2 - 1) + 1} \tag{18}$$

where

$$S(w) = \langle\psi^{w}_{\nu,m,i}|\psi_{N,m,i}\rangle = \int_0^\infty \rho\, d\rho\, \phi^*_{\nu,m}(\rho, w)\phi_{N,m}(\rho). \tag{19}$$

The orthogonality condition has to be satisfied. We note, however, that for states belonging to different subbands, the trial functions are obviously orthogonal. Within the same subband, trial wave functions with different m values are still orthogonal. Thus, only

those trial functions corresponding to levels with the same m in the same subband may not be exactly orthogonal. However, completely orthogonal wave functions can be constructed. For example, the $3p_{\pm1}$ and $4p_{\pm1}$ states are given by

$$|\psi_{3p_{\pm1}}\rangle = |\psi_{3p_{\pm1}}\rangle_0 - |\psi_{2p_{\pm1}}\rangle\langle\psi_{2p_{\pm1}}|\psi_{3p_{\pm1}}\rangle_0 \tag{20a}$$

$$|\psi_{4p_{\pm1}}\rangle = |\psi_{4p_{\pm1}}\rangle_0 - |\psi_{2p_{\pm1}}\rangle\langle\psi_{2p_{\pm1}}|\psi_{4p_{\pm1}}\rangle_0 - |\psi_{3p_{\pm1}}\rangle\langle\psi_{3p_{\pm1}}|\psi_{4p_{\pm1}}\rangle_0 \tag{20b}$$

where $|\psi_{2p_{\pm1}}\rangle$, $|\psi_{3p_{\pm1}}\rangle_0$ and $|\psi_{4p_{\pm1}}\rangle_0$ are written down according to (17).

As has been noted at the beginning of this paper, all Q2D hydrogenic states are identified by the standard bulk (3D) spectroscopic notation. As long as the donor ion remains at the well centre, states labelled by the set of quantum numbers (n, ℓ, m) evolve continuously either from the 2D limit (ν, m, i) as the well width increases indefinitely, or from the strong-field limit (N, m, i) as B decreases to zero, to the bulk (3D) states at $B = 0$. This method of labelling allows us to trace unambiguously a level from zero field to arbitrarily strong field in a quantum well. Hence the present variational method applies to the whole range of magnetic field strength. For easier reference, the correspondence of these three sets of quantum numbers for all levels up to $3d_{\pm2}$ and $4p_{\pm1}$ are listed in table 1.

Table 1. The correspondence between quantum number labels in different limits of Q2D hydrogenic impurity states.

3D bulk	2D (zero field) (ν, m, i)	3D (strong field) (N, m, i)
1s	(1, 0, 1)	(0, 0, 1)
2s	(2, 0, 1)	(1, 0, 1)
$2p_{-1}$	(2, −1, 1)	(0, −1, 1)
$2p_{+1}$	(2, +1, 1)	(1, +1, 1)
$2p_0$	(1, 0, 2)	(0, 0, 2)
3s	(3, 0, 1)	(2, 0, 1)
$3p_{-1}$	(3, −1, 1)	(1, −1, 1)
$3p_{+1}$	(3, +1, 1)	(2, +1, 1)
$3p_0$	(2, 0, 2)	(1, 0, 2)
$3d_0$	(1, 0, 3)	(0, 0, 3)
$3d_{-1}$	(2, −1, 2)	(0, −1, 2)
$3d_{+1}$	(2, +1, 2)	(1, +1, 2)
$3d_{-2}$	(3, −2, 1)	(0, −2, 1)
$3d_{+2}$	(3, +2, 1)	(2, +2, 1)
4s	(4, 0, 1)	(3, 0, 1)
$4p_{-1}$	(4, −1, 1)	(2, −1, 1)
$4p_{+1}$	(4, +1, 1)	(3, +1, 1)

With the wave function given by (17)–(20), the energy expectation value is then

$$\begin{aligned} E_{n,\ell,m} = \alpha[&E_{\nu,m,i} + \langle\psi^w_{\nu,m,i}|\tfrac{1}{4}\gamma^2\rho^2|\psi^w_{\nu,m,i}\rangle + \langle\psi^w_{\nu,m,i}|H'|\psi^w_{\nu,m,i}\rangle] \\ &+ \beta[E_{N,m,i} + \langle\psi_{N,m,i}|-(2/r)|\psi_{N,m,i}\rangle] \\ &+ 2\alpha\beta[E_{N,m,i}S(w) + \langle\psi^w_{\nu,m,i}|-(2/r)|\psi_{\nu,m,i}\rangle]. \end{aligned} \tag{21}$$

The variational principle is now applied to minimize the energy with respect to the two independent parameters, namely,

$$\partial E/\partial w = 0 \qquad \partial E/\partial\alpha = 0. \tag{22}$$

For a fixed magnetic field strength γ, equations (22) determine the variational parameters, which, in turn, determine the required energy level as a function of γ.

In our numerical calculation, we take the effective Bohr radius $a_0^* = \varepsilon_0\hbar^2/m^*e^2$ and the effective Rydberg $R^* = e^2/2\varepsilon_0 a_0^*$ as the units for the length and energy, respectively. The field strength is measured by the dimensionless quantity γ, the energy of the lowest Landau level in units of the effective Rydberg, defined by

$$\gamma = e\hbar B/2m^*cR^*. \tag{23}$$

The band gap difference in electronvolts is given by the empirical formula [25]

$$E_g = 1.1555x + 0.37x^2 \tag{24}$$

where x is the Al concentration in $Ga_{1-x}Al_xAs$, which is taken to be 0.3. The barrier height V_0 is taken to be 65% of the direct band gap difference between the barrier and the well. Other parameters adopted in the numerical work are listed in table 2 for all three samples of well width 125 Å, 210 Å and 450 Å. From these parameters, one converts γ to the magnetic field B in tesla by

$$\gamma = 0.148B. \tag{25}$$

Table 2. Parameters used in this work.

m_c^*/m_e	ε_0	R^* (meV)	a_0^* (Å)
0.067	12.5	5.83	98.7

Spectra of energy levels obtained this way are plotted in figure 1 as functions of the external magnetic field in the direction of growth. We have chosen the conduction band edge of bulk GaAs to be the zero point of the energy scale in these plots. For comparison purposes, Landau levels are also shown by the dashed lines in figure 1(a). The lowering of energy levels with increasing well width is apparent from these plots. Complications due to this weakening confinement will be discussed later. To provide data for quantitative comparison with other calculations, we display in table 3 the numerical results for 1s and $2p_{-1}$ states in wells of width $d = 125$ Å and 210 Å for magnetic field strengths up to about 30 T ($\gamma = 4.4$). It is remarked that the accuracy of our results improves with the increasing field.

4. Experimental details

The samples used in this experiment were cleaved from wafers grown by molecular beam epitaxy. Sample 1 consists of 30 GaAs wells of width 125 Å separated by $Al_{0.3}Ga_{0.7}As$ barriers of width 125 Å, and sample 2 consists of 20 GaAs wells of width 210 Å again separated by 125 Å width $Al_{0.3}Ga_{0.7}As$ barriers. Both samples were doped over the central one-third of the wells with Si donors at a nominal concentration of 1×10^{16} cm^{-3}. Sample 3 contains 15 GaAs wells of nominal width 450 Å separated by 125 Å width $Al_{0.23}Ga_{0.77}As$ barriers. Si donors were doped over the central one-third of these wells at a nominal concentration of 5×10^{15} cm^{-3}. The MQW structures were sandwiched between two AlGaAs

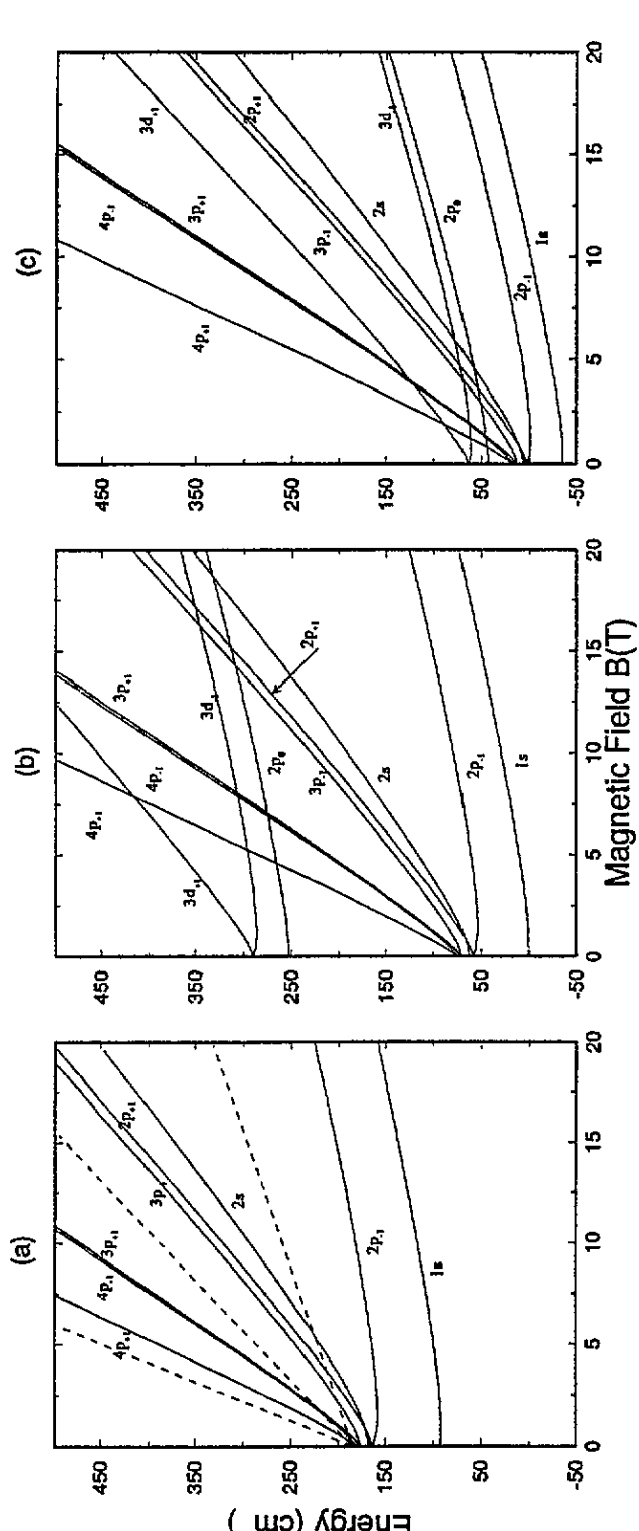

Figure 1. The variation of energy levels expressed as a function of the applied magnetic field for wells of different widths. The energy is measured from the GaAs conduction band edge of the MQW sample. For comparison purposes, we also plot in (a) the first four Landau levels as dashed lines, which merge at the first subband energy for zero field. (a) $d = 125$ Å; (b) $d = 210$ Å and (c) $d = 450$ Å.

Table 3. Energy levels of confined impurity for two different well widths as a function of the magnetic field. Energy levels are measured from the bottom of the conduction band of GaAs, in units of cm^{-1}.

		$D = 125$ Å		$D = 210$ Å	
γ	B (T)	1s	$2p_{-1}$	1s	$2p_{-1}$
0	0	91.79	163.13	0.837	58.02
0.2	1.351	92.16	158.61	1.371	53.84
0.4	2.703	93.90	159.46	3.689	55.11
0.6	4.054	96.77	162.09	7.284	58.07
0.8	5.405	100.49	165.66	11.66	61.93
1.0	6.757	104.81	169.85	16.50	66.39
1.2	8.108	109.56	174.46	21.63	71.33
1.4	9.459	114.55	179.49	26.95	76.65
1.6	10.810	119.77	184.80	32.48	82.29
1.8	12.162	125.13	190.40	38.15	88.17
2.0	13.513	130.63	196.18	43.99	94.28
2.2	14.865	136.27	202.16	49.98	100.63
2.4	16.216	142.01	208.32	56.10	107.07
2.6	17.567	147.89	214.62	62.35	113.70
2.8	18.918	153.86	221.06	68.70	120.47
3.0	20.270	159.93	227.64	75.19	127.39
3.2	21.622	166.09	234.32	81.82	134.35
3.4	22.973	172.39	241.09	88.54	141.45
3.6	24.324	178.74	247.96	95.36	148.64
3.8	25.675	185.18	254.87	102.23	155.88
4.0	27.027	191.72	261.92	109.23	163.22
4.2	28.378	198.30	269.03	116.29	170.65
4.4	29.729	204.98	276.17	123.44	178.13

layers of approximate width 1500–2000 Å. The entire structure was grown on a 2000 Å undoped GaAs buffer layer on a semi-insulating GaAs substrate and capped by a $\sim$ 100 Å GaAs layer [26].

A sensitive capacitively coupled photoconductivity technique was used to enhance the signal-to-noise ratio with respect to the conventional transmission measurements. In this technique, two semitransparent chromium electrodes separated by a small gap were evaporated on the top surface of the samples, and gold wires were attached to the chromium film electrodes by silver paint. At liquid helium temperatures the AlGaAs layer on top of the MQW structure acts as an insulator, and the doped GaAs wells, due to photothermal ionization of impurities, act as a set of parallel photosensitive resistors. A low-frequency ($\sim$ 100 Hz) AC voltage was applied between the two metal electrodes coupled capacitively to the resistively conducting quantum well plates, and the AC through the sample (in plane) was detected.

Far-infrared (FIR) magneto-optical spectra were obtained by using a repetitive slow-scan Fourier transform spectrometer, and light pipe and light cone optics in conjunction with a 9 T superconducting magnet. All data were taken at liquid helium temperatures and in the Faraday geometry, in which the magnetic field was parallel to the FIR light propagation direction and normal to the sample surface.

Figure 2 shows typical photothermal ionization spectra for samples 1 and 3 at several magnetic fields. Identified transitions are indicated by dashed lines in the figure. For sample 1, the most prominent peak at zero field has been identified as $1s \rightarrow 2p_{\pm 1}$ transitions degenerate at $B = 0$. This feature splits into $1s \rightarrow 2p_{+1}$ and $1s \rightarrow 2p_{-1}$ peaks as the field

increases, which behaviour is well known. In addition to these strong transitions, two weaker features at higher frequencies can be distinguished due to the sensitivity of the photothermal ionization technique. These features move to higher frequencies much more rapidly than the $1s \rightarrow 2p_{+1}$ transition as the field increases. These lines have been identified as $1s \rightarrow 3p_{+1}$ and $1s \rightarrow 4p_{+1}$ transitions based on considerations of the 3D $\rightarrow$ 2D and low-field–high-field correspondences, as well as selection rules of the transitions.

For sample 3, data at fields below 2 T are rather difficult to obtain due to the nature of the photoconductive process because smaller binding energy leads to a larger number of thermally excited conducting electrons, which masks the photoexcitations. At higher fields this sample shows two additional features indicated as A and B. Both of them are very weak and become observable only when the spectra are expanded. It seems that these lines have the same slope as the $1s \rightarrow 2p_{+1}$ transition. Therefore the final states are both associated with the $N = 1$ Landau level. From the selection rules for the allowed dipole transition, line A is identified as the $1s \rightarrow 3p_{-1}$ transition for which there is no theoretical curve for comparison. Further calculation is needed to study these lines in more detail.

Transition energy measurements as described above have been carried out for all three samples. Results are compared with theoretical curves in figure 3. It is observed that the agreement is generally good for all the measured transitions in cases (a) and (b). For the 450 Å well, the calculated results are consistently lower than experimental data as can be seen in (c). The discrepancies are sizeable, but are not surprising because the variational trial functions are constructed under the assumption of strong confinement and are expected to deteriorate with increasing well width.

5. Discussion

We have investigated the energy levels and transition energies of Q2D impurity atoms in a quantum well of fixed width as functions of the applied magnetic field. Our trial wave functions yield correct levels at zero field and in the high-field limit. It is observed from figure 1 that energy levels with the same quantum number n are degenerate at $\gamma = 0$, and split due to the Zeeman effect just like 2D hydrogenic states. On the other hand, we see that energy levels form groups according to Landau index in the high-field region. For example, $2p_{+1}$ and $3p_{-1}$ belong to the same Landau level and they have the same field dependence as the field becomes strong.

A careful examination of the theoretical results reveals that the separation between levels that belong to the same Landau index decreases with increasing excitation. For instance, the energy difference between 1s and $2p_{-1}$ is larger than that between $2p_{+1}$ and $3p_{-1}$, which in turn is larger than that between $3p_{+1}$ and $4p_{-1}$, etc. A similar situation occurs when we look at the level separation in different subbands. For example, the level separation of the lowest pair 1s and $2p_{-1}$ in the first subband is larger than that of the lowest pair $2p_0$ and $3d_{-1}$ in the second subband. This phenomenon may be easily understood from the fact that the energy separation originates from the Coulomb energy in different impurity states. Since higher excited states tend to spread out more than the lower states, the perturbation due to Coulomb interaction decreases with increasing excitation.

Let us now turn our attention to the behaviour of the 2s level. Figure 1 shows that this level starts higher than $2p_{+1}$ at zero field and becomes lower than $2p_{+1}$ at high fields. Although no data exists on transitions involving the 2s level, the level crossing is, to some extent, expected by considering wave functions in the two limits. The 2D hydrogenic 2s and $2p_{\pm 1}$ are degenerate when $\gamma = 0$. The 2s wave function is more extended than $2p_{\pm 1}$

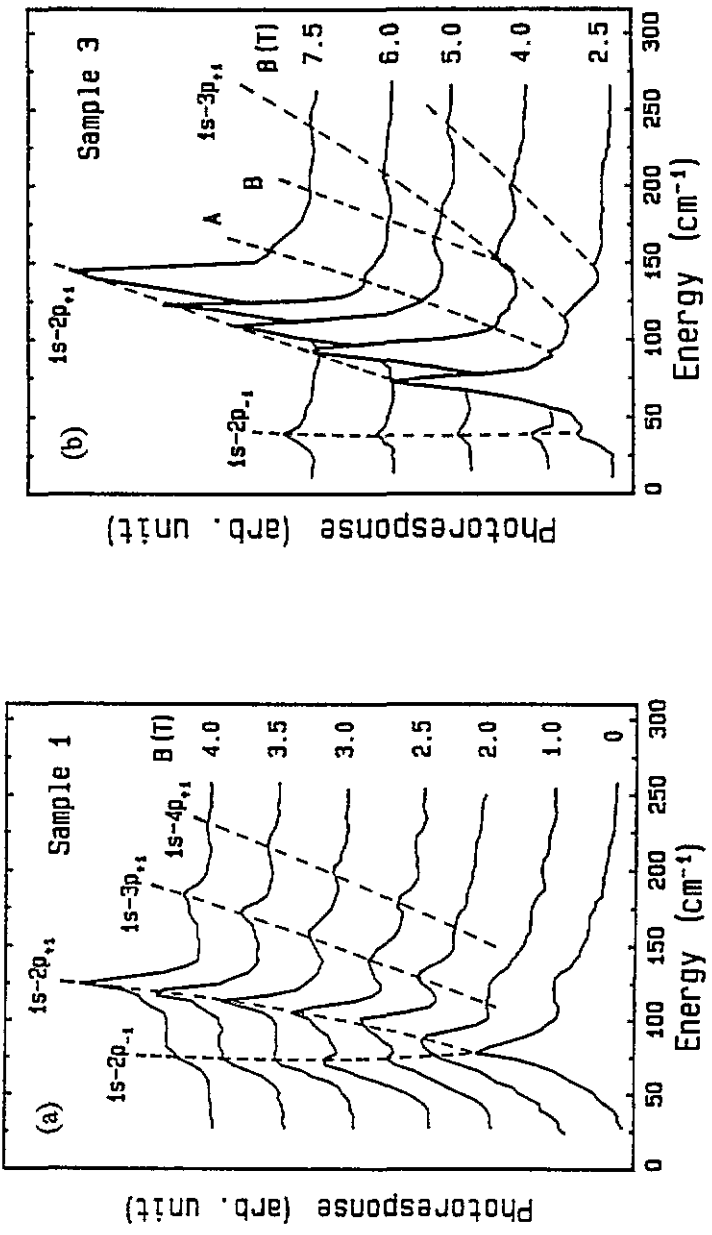

Figure 2. Capacitively coupled photoconductivity spectra of impurity transitions for (a) sample 1 ($d = 125$ Å) and (b) sample 3 ($d = 450$ Å) at several magnetic fields and at liquid helium temperatures. The 'shoulder' in (a) at ~ 120 cm^{-1} in the zero-field spectrum is an artifact from multiple-internal-reflection interference in a white polyethylene window in the light pipe system, not the $1s \rightarrow 3p_{+1}$ or $1s \rightarrow 4p_{+1}$ transition.

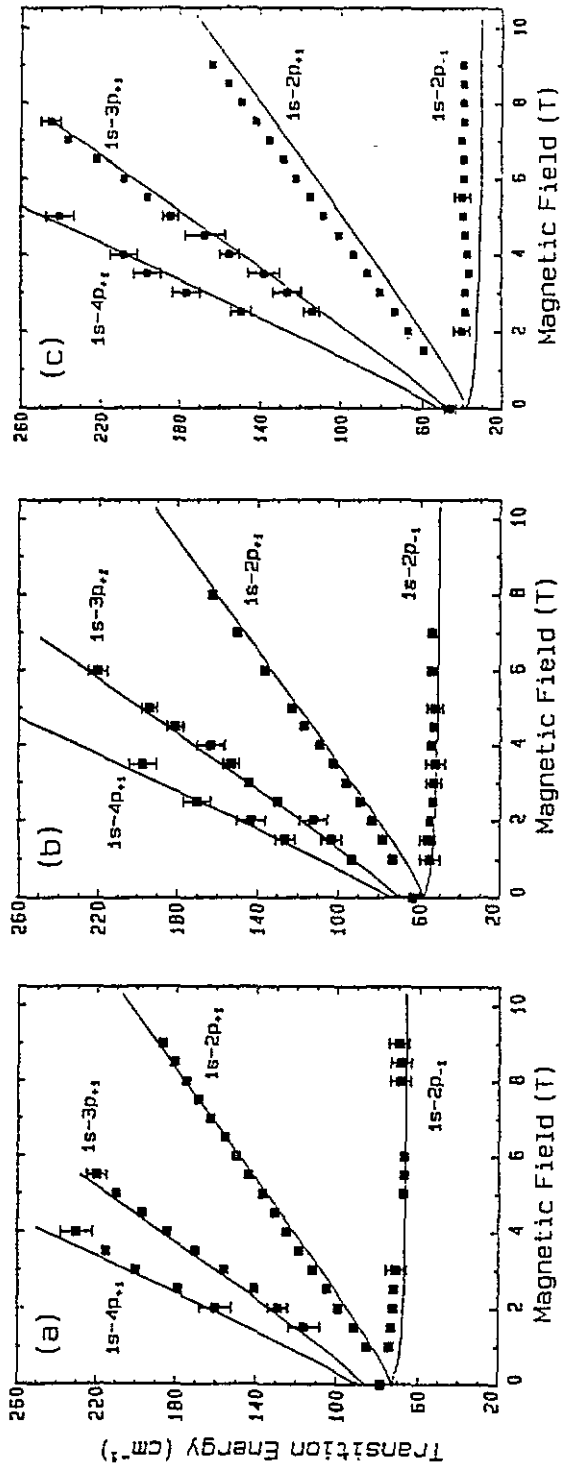

Figure 3. $1s \rightarrow np$ transition energies as functions of the applied magnetic field for different well widths: (a) $d = 125$ Å; (b) $d = 210$ Å and (c) $d = 450$ Å. The squares are measured data and lines are calculated results. The final state of each transition is marked next to the line.

wave functions. When the perturbation H' is included, therefore, $2p_{\pm1}$ levels become lower than 2s due to the 2D and 3D potential energy difference. On the other hand, 2s and $2p_{+1}$ levels have the same Landau index N, hence they increase with increasing field with the same slope in the strong-field limit, but they have different m values. The 2s wave function extends less than $2p_{+1}$ in the xy plane at high fields. Therefore the Coulomb potential correction brings the 2s level below $2p_{+1}$.

For $1s \rightarrow 3p$ and $1s \rightarrow 4p$ transitions, the curves in figure 3 appear to deviate from data at the high-field end. This is the result of electron–phonon interactions near the resonance region as has been shown in our previous investigations of the $1s \rightarrow 2p_{+1}$ transition [27, 28]. There is no observable deviation in the region of field strength under consideration for $1s \rightarrow 2p_{\pm1}$ transitions because the resonance occurs at very high magnetic field (~ 16 T).

Effects of confinement are studied by considering wells of different widths; it is interesting to see how these transition energies change with the well width for fixed magnetic fields. In figure 4, we plot some of the energy levels calculated as functions of the well width for (a) zero field and (b) $B = 20.3$ T. The effect of confinement is perhaps best illustrated by following the change of the 2p levels with the decreasing width. At zero field, these levels are degenerate in the bulk. The quantum confinement splits $2p_0$ from $2p_{\pm1}$, which remain degenerate as shown in figure 4(a).

For the sake of illustration, it is convenient to define a quantity $\Delta = [E(2p_0) - E(2p_{\pm1})]/E(2p_{\pm1})$, which may be regarded as a measure of the quantum confinement of this particular case. At $d = 300$ Å, figure 4(a) shows $\Delta \approx 1$. Hence we expect that the strong-confinement approximation yields good results for $d \lesssim 300$ Å. At $d = 450$ Å, on the other hand, we find from our numerical work $\Delta \lesssim 0.1$. Therefore the strong-confinement assumption cannot be very reliable in this case. As a consequence, transition energies calculated for $d = 450$ Å cannot be as accurate as those for narrower widths. As d decreases further, it becomes clear that the $2p_0$ level behaves more like $3d_{+1}$. In fact, $2p_0$, $3p_0$ and $3d_{\pm1}$ belong to the second subband according to table 1 while $2p_{\pm1}$ along with the s levels remain in the first subband. All the energy levels rise when the quantum well narrows down as expected. Since all subbands higher than the first are pushed up as the well narrows, table 1 provides a clear picture to explain the different energy level schemes for 2D and 3D hydrogenic atoms.

Figure 4(b) illustrates the situation when the magnetic field $B = 20.3$ T. The degeneracy of $2p_{\pm1}$ is lifted by the field, and the $2p_{+1}$ level crosses over $2p_0$ and $3d_{-1}$ at about $d = 230$ Å and 245 Å, respectively. Because of the crossover of levels from different subbands, strong subband mixing is expected for quantum wells of large width. Therefore the discrepancies observed in figure 3(c) should be improved by including the subband mixing in the trial wave functions.

Theoretical results can in general be improved somewhat by including the non-parabolicity effects on the effective mass, which is taken in the present calculation as the band edge mass. This correction generally lowers the high-field results and raises the low-field results, each by a couple of wave numbers. There are of course other minor corrections that may be considered in any future work along this line. For instance, we have assumed equal effective masses and identical dielectric constants for both GaAs and AlGaAs. We believe, however, that these factors would not result in any qualitative change but would complicate the calculation considerably.

From the above discussion, it is clear that the variational method proposed here is especially good for well widths $d \lesssim 300$ Å. Under this condition, the electronic states are highly confined, so that the approximate factorization of the subband wavefunction $f_i(z)$ from the in-plane wave function is valid. For larger well widths, however, the separation

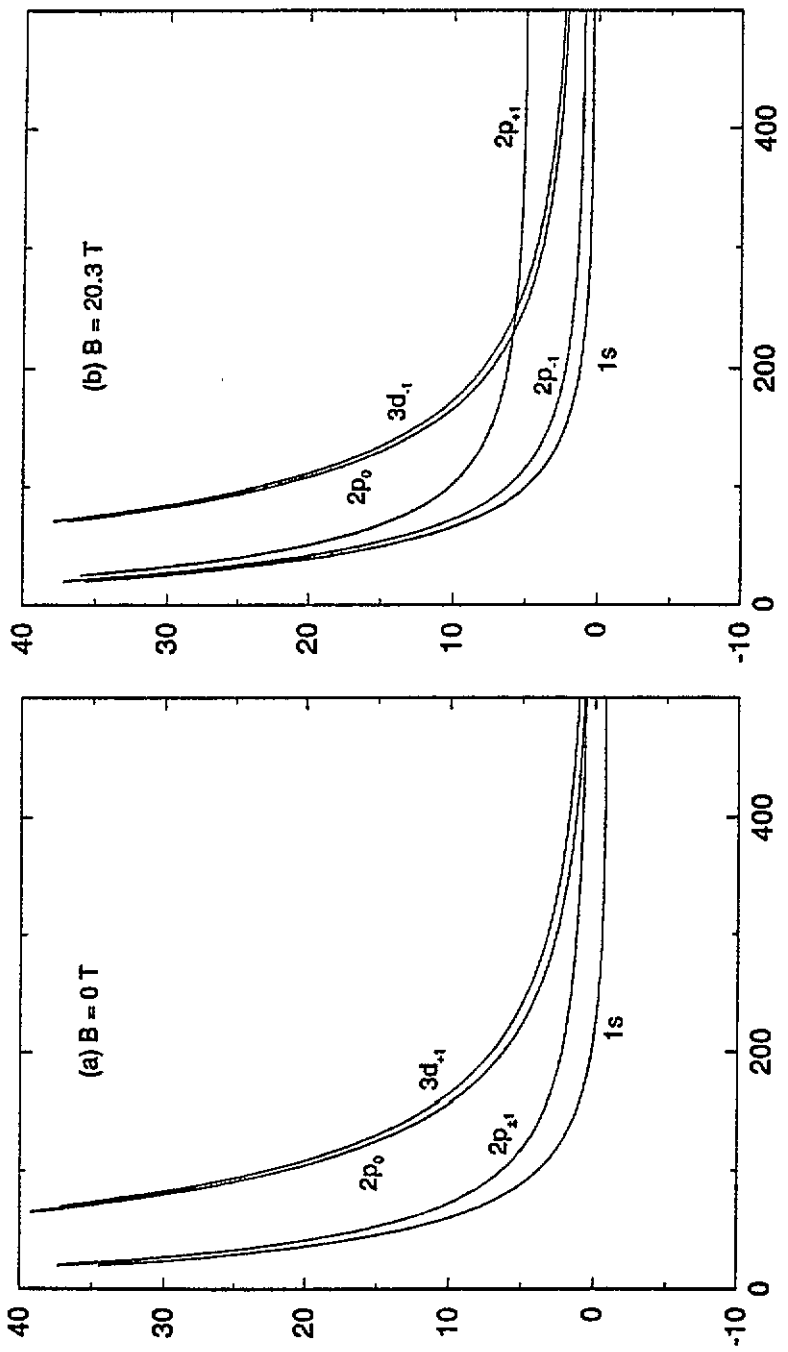

Figure 4. The change of Q2D energy levels with the well width for a fixed magnetic field. (a) $B = 0$ and (b) $B = 20.3$ T.

between different subbands can be smaller than the Rydberg constant. Consequently, the mixing between the levels belonging to different subbands becomes so frequent that this approach breaks down. Therefore, the validity of the present theory may be roughly set by the condition that the subband energy separation $\Delta E_i > R^*$. For $GaAs/Al_xGa_{1-x}As$ quantum wells, this gives a rough upper bound of the well widths of ~ 600 Å.

Acknowledgment

This work was supported in part by the Office of Naval Research.

References

[1] Lee Y C and Lin D L 1979 *Phys. Rev.* B **19** 1982
[2] Bastard G 1981 *Phys. Rev.* B **24** 4714
[3] Chaudhuri S 1983 *Phys. Rev.* B **28** 4480
[4] Mailhiot C, Chang Y C and McGill T C 1982 *Phys. Rev.* B **26** 4449
[5] Greene R L and Bajaj K K 1983 *Solid State Commun.* **45** 825
[6] Chaudhuri S and Bajaj K K 1984 *Phys. Rev.* B **29** 1803
[7] Tanaka K, Nagaoka M and Yambe T 1983 *Phys. Rev.* B **28** 7068
[8] Greene R L and Bajaj K K 1985 *Phys. Rev.* B **31** 913
[9] Jian-Lin Zhu 1989 *Phys. Rev.* B **40** 10529
[10] Wen-Ming Liu and Quinn J J 1985 *Phys. Rev.* B **31** 2348
[11] Jarosik N C, McCombe B D, Shanabrook B V, Comas J, Ralston J and Wicks G 1985 *Phys. Rev. Lett.* **54** 1283
[12] Makado P C and McGill N C 1986 *J. Phys. C: Solid State Phys.* **19** 873
[13] Aldrich C and Greene R L 1979 *Phys. Status Solidi* b **93** 343
[14] Armstead C J, Stradling R A and Wasilewski Z 1989 *Semicond. Sci. Technol.* **4** 557
[15] Klarenbosch A V, Klaassen T O and Wenckeboch W Th 1990 *J. Appl. Phys.* **67** 6323
[16] Stopa M and DasSarma S 1989 *Phys. Rev.* B **40** 8446
[17] MacDonald A H and Ritchie D S 1986 *Phys. Rev.* B **33** 8336
[18] Zhu J L, Cheng Y and Xiong J J 1990 *Phys. Rev.* B **41** 10792
[19] Larsen D M 1991 *Phys. Rev.* B **44** 5629
[20] Dunn J L and Pearl E 1991 *J. Phys. C: Solid State Phys.* **3** 8605
[21] Chen R, Cheng J P, Lin D L, McCombe B D and George T F 1991 *Phys. Rev.* B **44** 8315
[22] Cheng J P and McCombe B D 1990 *Phys. Rev.* B **42** 7626
[23] Dingle R B 1952 *Proc. R. Soc.* A **211** 500
[24] Lee N, Larsen D M and Lax B 1973 *J. Phys. Chem. Solids* **34** 1059
[25] Lee H J, Juravel L Y, Wolley J C and Springthorpe A J 1980 *Phys. Rev.* B **21** 659
[26] Cheng J P and McCombe B D are grateful to J Ralston and G Wicks for the growth of samples 1 and 2 at Cornell University and to B V Shanabrook for providing them with sample 3, which was grown by J Comas at NRL
[27] Cheng J P, McCombe B D and Brozak G 1991 *Phys. Rev.* B **43** 9324
[28] Lin D L, Chen R and George T F 1991 *Phys. Rev.* B **43** 9328